15th Australasian Fluid Mechanics Conference
The University of Sydney, Sydney, Australia
13-17 December 2004

Surface-Flow Patterns in Oscillating-Triangular-Jet Nozzles

S. K. Lee, P. V. Lanspeary, G. J. Nathan and R. M. Kelso

School of Mechanical Engineering
The University of Adelaide, Adelaide, South Australia, 5005 AUSTRALIA

Abstract

A triangular-jet nozzle which usually produces an oscillating-jet flow can, for a narrow range of geometric parameters, produce a stationary deflected jet which reattaches to the internal surface of the nozzle. Surface-flow-visualisation images and surface-pressure maps from the stationary deflected jet contain a wealth of detail not available from similar experiments with the oscillating-jet flow. In the topological model constructed from this data, the most significant feature is a strong sink focus. The model suggests that most of the reverse flow through exit plane of the nozzle is attracted towards this sink focus before it is entrained by the jet flow and ejected from the nozzle.

Introduction

Nathan et al. [5] have shown that a nozzle consisting of a circular inlet orifice and a chamber with an exit lip can produce a naturally oscillating jet flow. This device is known as the "fluidic-precessing-jet" (FPJ) nozzle because flow from the inlet orifice reattaches asymmetrically to the wall of the chamber. In the absence of a preferred azimuthal orientation, the reattaching flow "precesses" around the wall (Figure 1).

At an early stage, the FPJ nozzle was developed as an industrial natural-gas burner because the flame is shorter, more luminous and more resistant to "blow-off" than equivalent simple-turbulent-jet or "axial-jet" nozzles [6]. The higher luminosity can lead to a decrease of up to about 40% in nitrogen-oxide (NO_x) emissions [7].

Nathan et al. [5] have also shown that, for reliable oscillation of the jet flow, the expansion ratio of the inlet-orifice diameter (D/d_1) must be larger than 5.0, and length-to-diameter ratio of the chamber (L/D) must be in the range $2.60 < L/D < 2.80$. Of these geometric criteria, the requirement for a small inlet orifice ($D/d_1 \geq 5.0$) makes the fuel supply pressure much higher than for an axial-jet burner of the same outer diameter and (heat) capacity. This can be a costly problem if the supply pressure is inadequate; either the pressure must be increased or the burner must be larger.

Mi et al. [4] found that, if the inlet-orifice shape is changed from circular to triangular, jet oscillation occurs at orifice area expansion ratios as low as 4.0. For a fixed burner capacity, this allows either a reduction in supply pressure by an order of magnitude or a reduction of the nozzle diameter by a factor of about two.

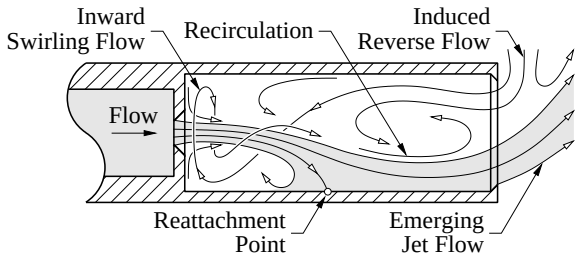

Figure 1: Schematic flow-field pattern for the "fluidic-precessing-jet" (FPJ) nozzle inferred from visualisation [5].

Lee et al. [3] have performed a parametric study of the "oscillating-triangular-jet" (OTJ) nozzle. Their results verify that oscillations occur at much smaller expansion ratios than in the FPJ and that, unlike an FPJ, oscillation is continuous rather than intermittent. In comparison with the FPJ, the jet spreading angle is smaller and varies more gradually over a wide range of L/D ratios and inlet-expansion ratios. This provides a capacity, by selecting appropriate L/D and inlet-expansion ratio, to design a nozzle with not only a much lower supply pressure than the FPJ nozzle, but also with a selectable jet spreading angle.

This paper reports the results of surface-flow-visualisation experiments. These are the first investigations of large-scale flow structure inside the OTJ nozzles.

Experimental Technique

Figure 2 shows the oscillating-jet nozzle used for this investigation. Flow enters the nozzle chamber, which has an internal diameter D, through an equilateral triangular inlet-orifice plate and it leaves the chamber through an exit lip of diameter $d_2 = 0.9D$. There are four available inlet orifices with area expansion ratios of $(D/d_{e1})^2 = 2.1^2$, 2.5^2, 3.0^2 and 3.5^2, where d_{e1} is the "equivalent diameter" of the triangular orifice. The length of the chamber can be adjusted to any value within the range $0.00 \leq L/D \leq 3.00$. To permit visualisation of the internal flow, the chamber is made of Perspex tube.

The nozzle is connected to a compressed-air supply through a straight tube of diameter $D_0 = 0.763D$ and length $50D_0$. At the upstream end of the tube is a flow conditioner consisting of a

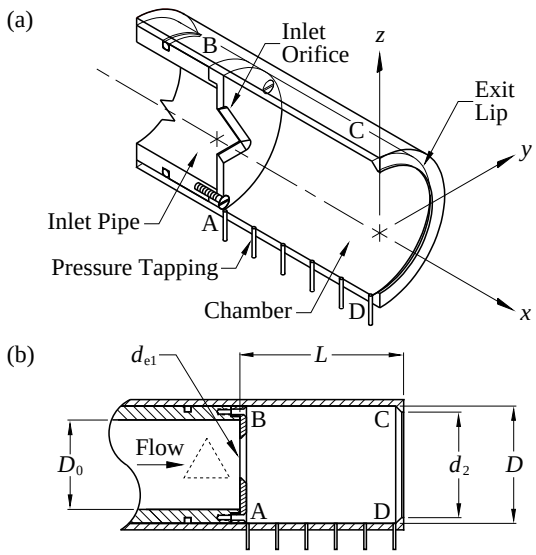

Figure 2: The "oscillating-triangular-jet" (OTJ) nozzle (a) components and (b) geometric parameters.

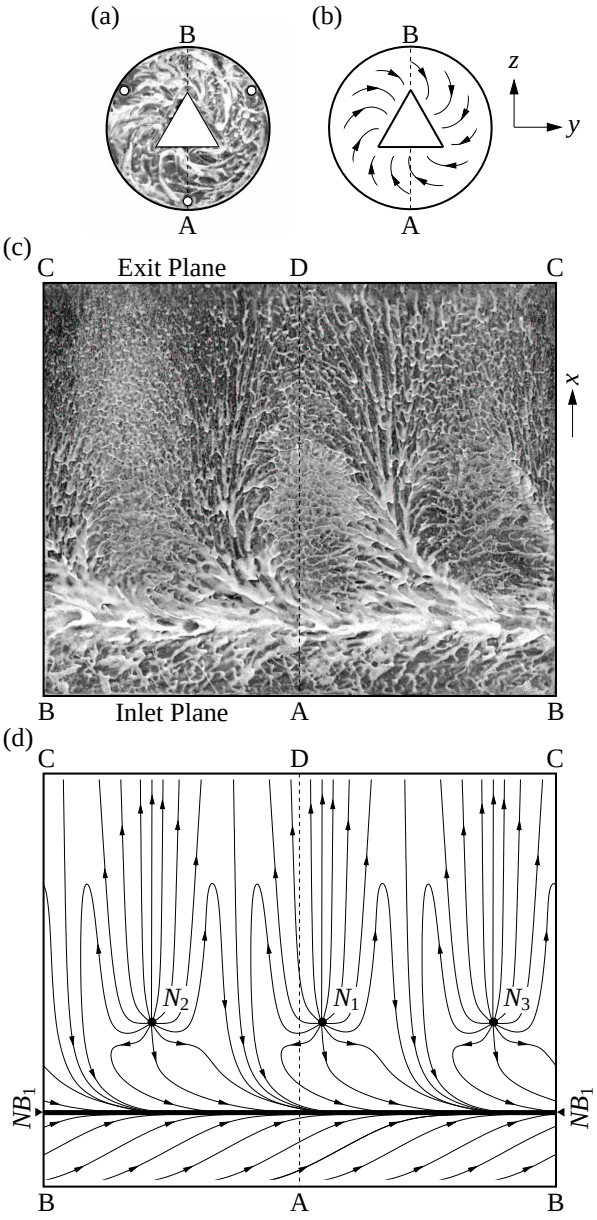

Figure 3: Oscillating triangular jet surface-flow visualisation pattern and streakline interpretation; (a, b) inlet plane, (c, d) cylindrical surface. $D/d_{e1} = 3.5$ and $L/D = 2.50$ at $Re_1 = 70,000$.

"honeycomb" (of plastic drinking straws) followed by a wire-mesh screen. Further details of the flow conditioning and of the ancillary equipment are provided by Lee et al. [3].

The method of flow visualisation is similar to the "china-clay" technique described by Bradshaw [1] and adopted by Nathan et al. [5] for investigating the surface-flow patterns in the FPJ nozzle. A transparent A4-size plastic sheet, 0.1 mm thick, is cut to the internal length and circumference of the nozzle chamber, and is then inserted so that it forms a new inner surface of the chamber. A viscous mixture of white toothpaste, cornflour and water is painted uniformly onto the plastic sheet and is immediately exposed to the flow until the water evaporates (which takes about 12 minutes). To record the "streakline" pattern produced by the flow, the plastic sheet is removed from the nozzle and unrolled. Four "streakline" images were obtained for each flow condition. While the flow is producing a pattern on the plastic sheet, it also spreads paste over the back face of

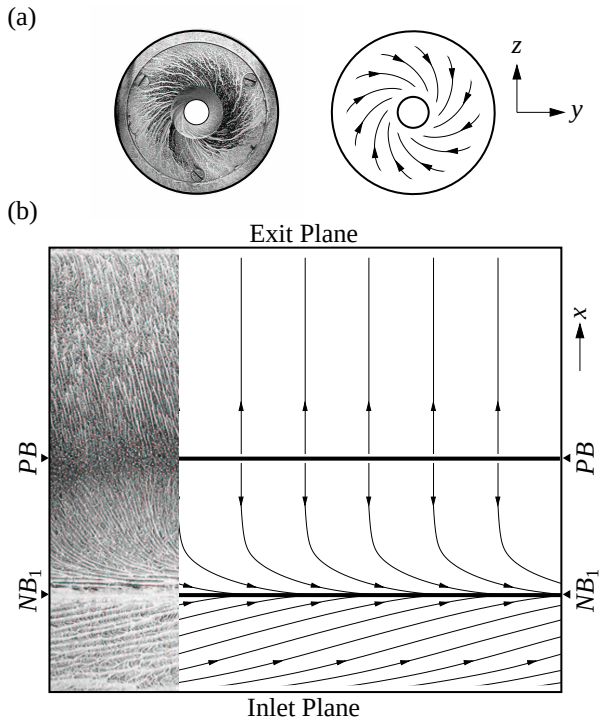

Figure 4: Fluidic precessing jet surface-flow visualisation pattern and streakline interpretation; (a) inlet plane, (b) cylindrical surface [5]. $D/d_{e1} = 6.4$ and $L/D = 2.70$ at $Re_1 = 280,000$.

the chamber. The pattern thus formed on the inlet-orifice plate is also recorded as an image.

The flow visualisation is supplemented by measurements of static pressure from a row of six pressure tappings through the wall of the chamber (Figure 2). The distance between tappings is $D/4$. An azimuthal increment of 30° is obtained by rotating the chamber about its axis. For each measurement the signal from the pressure transducer was time averaged for 100 seconds on a digital oscilloscope.

Oscillating-Jet Flows

The flow-visualisation patterns and corresponding surface-streakline interpretations for the OTJ nozzle are shown in Figure 3. The expansion ratio is $D/d_{e1} = 3.5$ and the chamber length is $L = 2.50D$. The other expansion ratios (2.1, 2.5 and 3.0) produce similar flow patterns.

The spiral pattern in Figure 3(a), which indicates a radially inward swirling flow at the inlet plane, is similar to that observed by Nathan et al. [5] in the FPJ nozzle (Figure 4(a)). In the interpretation of the flow field, this swirling flow (Figure 3(b)) is entrained into the flow from the inlet orifice.

In the OTJ nozzle, flow from the inlet orifice is deflected asymmetrically and reattaches to the cylindrical surface of the chamber. Azimuthal (or tangential) motion of the reattachment point appears as oscillation of the jet. Lee et al. [3] have shown that the preferred locations for the reattachment point are aligned azimuthally at midway between corners of the orifice. In Figures 3(c) and 3(d), these preferred locations are shown as nodes N_1, N_2 and N_3. In surface-flow visualisation of the FPJ nozzle [5], the moving reattachment point has no preferred direction and appears as a positive bifurcation, line PB in Figure 4(b).

The strongest feature in the OTJ flow-visualisation pattern (Figure 3(c)) is a circumferential "ring" (NB_1) where converging

flow has caused a build-up or thickening of the paste. Nathan et al. [5] interpreted a similar feature in flow-visualisation patterns (Figure 4(b)) from the FPJ nozzle as a negative-bifurcation line. Surface-flow streaklines consistent with the flow-visualisation pattern of Figure 3(c) are drawn in Figure 3(d). These streaklines may approximate a time-average of flow in the OTJ nozzle but, like Figure 4(b), they do not provide much insight into the mechanism of the flow.

Stationary-Deflected-Jet Flow

The behaviour of the flow in the OTJ nozzle and the behaviour of the jet emerging from the exit plane depend on expansion ratio (D/d_{e1}), length (L/D), and Reynolds number (Re_1). In their parametric study, Lee et al. [3] found that, with $L/D \leq 1$, the flow from the inlet orifice remains axisymmetric, and there is no large-scale oscillation. For L/D between 1.25 and 3.00, the jet oscillates in a manner which produces the flow-visualisation pattern of Figure 3(c).

However, these are not the only flow regimes of the OTJ. For a very narrow range of "critical" values near $L/D = 1.25$, Lee et al. [3] observed that the jet from the "$D/d_{e1} = 3.5$" orifice is deflected towards the wall, but does not oscillate. Increasing chamber length beyond this narrow but critical L/D range causes the deflected jet to oscillate. We would therefore expect a flow pattern produced by the stationary (or non-oscillating) jet to be related to the phase-averaged flow of an oscillating jet. Figure 5 shows that the surface-flow visualisation pattern for the stationary deflected jet is significantly different from the visualisation pattern for the oscillating jet. The most striking difference between Figure 5(c) and Figure 3(c) is that the built-up line of paste representing the negative-bifurcation line NB_1 is no longer straight.

To assist with the interpretation of the flow-visualisation pattern we have measured the distribution of time-averaged static pressure on the internal cylindrical surface of the nozzle. This is presented in Figure 5(d) as contours of static-pressure coefficient, $C_p = p_s/q_1$, where p_s is the wall static pressure and q_1 is the mean dynamic pressure of flow through the inlet orifice. The location of maximum pressure, shown as the $C_p = 0.00$ contour, is the reattachment "point" of the deflected jet. In Figure 5(e), this is the "source" node N_1. Closer to the inlet plane and to each side of the pressure maximum, there is a region of minimum pressure ($C_p = -0.13$). These coincide with large accumulations (or "blobs") of paste in the flow-visualisation image (Figure 5(c)). Clearly observed rotation of the larger "blob" implies there is a "sink" focus at the corresponding pressure minimum. This is shown as F_1 in Figure 5(e). The smaller "blob" is represented by focus F_2. The existence of saddles S_1 and S_2 is deduced from the rules of topology.

In the experiment (Figure 5(c)), paste spreads to the left and to the right of the reattachment node, N_1. Flow spreading to the left of N_1 is drawn into focus F_1 and flow spreading to the right is drawn into the negative-bifurcation line NB_1. Features F_1 and NB_1 are strong sinks where flow separates from the surface and they also induce a reversed flow through the exit plane (Figure 5(e)). Since the surface is cylindrical, and is continuous along the left and right edges of the diagram, flow which spreads circumferentially away from N_1 must also converge towards a negative bifurcation which extends from the exit plane and into focus F_1. This negative bifurcation is shown in Figure 5(e) as the line NB_2. The complementary positive-bifurcation line PB_1 extends from node N_1 to the exit plane.

The strongly swirling surface flow between the inlet plane and NB_1 (Figure 5(e)) is directed away from the edge $\overline{\text{BAB}}$. The inward-spiral flow-visualisation pattern in Figure 5(b) also indicates flow directed away from the perimeter $\overline{\text{BAB}}$, and so continuity requires a positive-bifurcation line between the inward-spiral flow and the flow on the cylindrical surface. The positive bifurcation is shown in Figure 6(a) as the closed loop PB_2. In the side view, Figure 6(b), the positive bifurcation (PB_2) is visible as saddles S_3 and S_4. A topologically consistent side-view flow pattern (Figure 6(b)) is obtained by placing foci F_3 and F_4 in the swirling near-surface flow, and F_5 in the recirculation region between the reattachment point S_7 and the inlet plane [8].

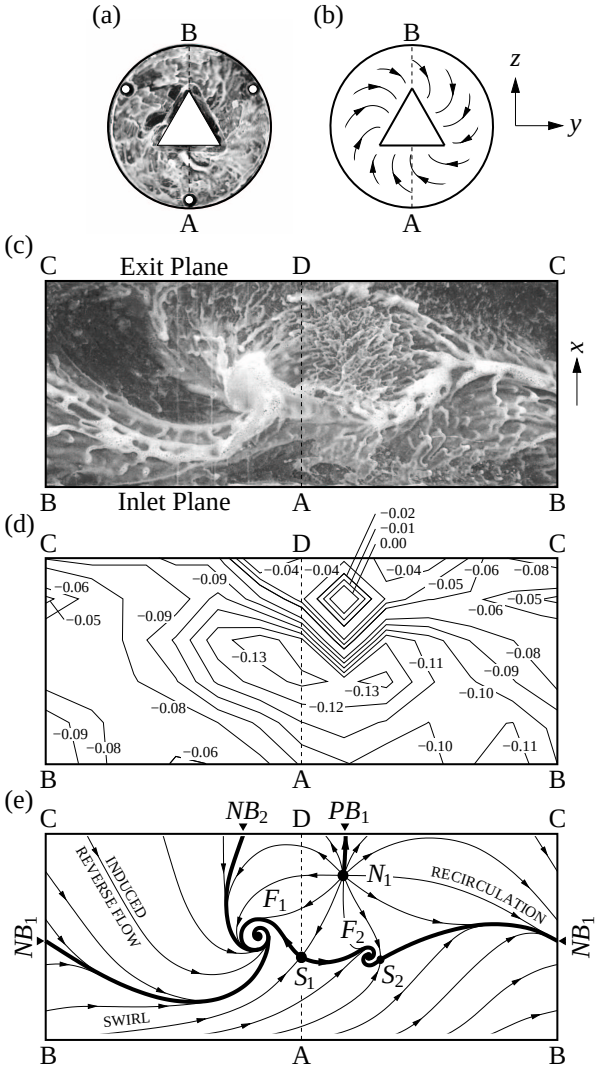

Figure 5: Surface-flow visualisation of the stationary deflected jet; (a, b) inlet plane, (c) cylindrical surface, (d) distribution of static-pressure coefficient, C_p, (e) streakline interpretation. $D/d_{e1} = 3.5$ and $L/D = 1.25$ at $Re_1 = 70,000$.

Flow at the Exit Plane

There are two regions of flow at the exit plane, the emerging-jet-flow region, and the induced-reverse-flow region. The contour plots in Figure 7 are of the time-averaged signal from a total-pressure tube (i.e. Pitot probe) placed sequentially at each of 241 points distributed over the exit plane of the nozzle. The results are plotted as a pressure coefficient based on q_1, the dynamic pressure at the inlet orifice. The Pitot probe is aligned parallel to the axis so that, when placed in the emerging jet flow, it provides an approximate measurement of jet-flow speed. When the probe is placed in the induced-reverse-flow region, the recorded pressure is *negative*.

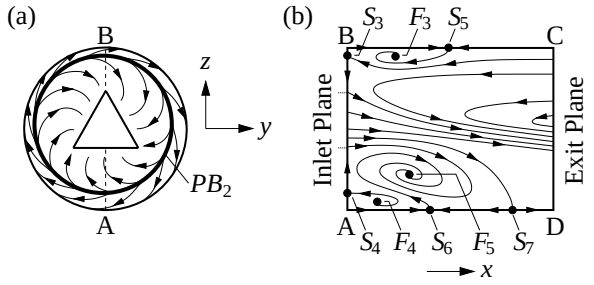

Figure 6: Flow topology of the stationary deflected jet in the oscillating-triangular-jet nozzle; (a) inlet plane, (b) azimuthal plane $\overline{\text{ABCD}}$.

Figure 7 shows that only an outer part of the jet shear layer reattaches to the side wall of the nozzle. The higher velocity part of the emerging jet ($0.20 \leq C_\text{p} \leq 0.80$) is deflected by only a small amount ($\approx D/9$) and discharges from the exit plane without interacting directly with the wall of the nozzle.

We propose the following model for flow near the reattachment node N_1. Focus F_1 (Figure 5(e)) is the end of a line vortex which extends away from the internal surface of the OTJ nozzle. The vortex beginning at F_1 is a feature of the turbulent shear layer of the deflected-jet flow and, as indicated by $\overline{F_1F_6}$ in Figure 8(a), it is drawn out of the OTJ chamber as a longitudinal vortex aligned with the axis of the nozzle. The weaker vortex beginning at F_2 is also entrained and drawn out of the chamber on the other "side" of the deflected jet. As suggested by the Kelso model of the FPJ [2], the vortex F_5 (Figure 6(b)) would be entrained by the jet flow so that it is stretched into the form of a horseshoe vortex. In Figure 8(b), the stretched legs of the horseshoe vortex are combined with the "legs" of the $\overline{F_1F_6}$ and $\overline{F_2F_7}$ vortices. This leads to a sketch of the non-axial components of the flow at the exit plane (Figure 8(b)). Saddle S_8 corresponds to the positive bifurcation PB_1 of Figure 5(e), and saddle S_9 corresponds to the negative bifurcation NB_2.

Conclusions

From flow visualisation and static-pressure measurements at the internal surface of the OTJ nozzle, the authors have identified a number of bifurcation lines and critical points in the stationary-deflected-jet flow observed by Lee et al. [3]. These are shown in Figures 5(e), 6 and 8(b). Although deflection of the jet centreline is only about $D/9$, there is a clearly observed reattachment node downstream of the inlet plane (or backward-facing step). Closer to the inlet plane and to each side of the reattachment node, flow separates from the surface at a strong sink focus, F_1, and a much weaker focus F_2. The surface-flow pattern indicates that much, and perhaps most of the reverse flow through the exit plane of the nozzle is attracted towards F_1. A rather distorted circumferential negative bifurcation NB_1 also flows into F_1. The vortices which terminate at F_1 and F_2 are features of the shear layer in the reattached flow, and so they are drawn through the exit plane as longitudinal counter-rotating vortex "legs".

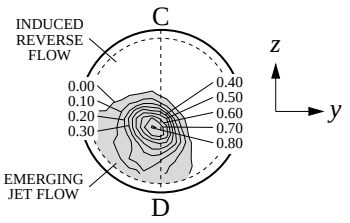

Figure 7: Stationary deflected jet at the nozzle exit plane; distribution of Pitot-pressure coefficient, C_p. $D/d_{e1} = 3.5$ and $L/D = 1.25$ at $Re_1 = 70,000$.

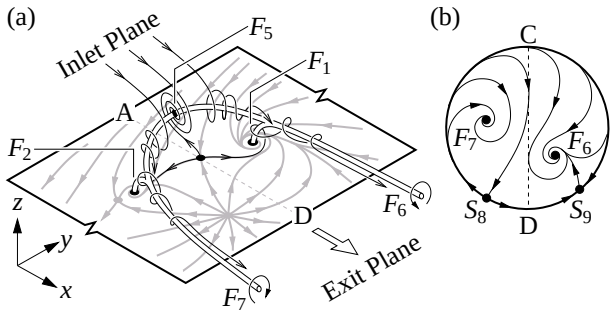

Figure 8: Stationary deflected jet; (a) "vortex skeleton" compatible with the foci in Figures 5 and 6, (b) schematic streamline pattern of in-plane velocity components at the nozzle exit plane.

A topologically consistent model of flow between NB_1 and the inlet plane is obtained by placing a positive-bifurcation loop on the back face of the nozzle.

References

[1] Bradshaw, P., *Experimental fluid mechanics*, Pergamon Press Ltd., Oxford, 1970.

[2] Kelso, R. M., A mechanism for jet precession in axisymmetric sudden expansions, in *Proceedings of the Fourteenth Australasian Fluid Mechanics Conference*, The University of Adelaide, Adelaide, Australia, 2001, 829–832.

[3] Lee, S. K., Lanspeary, P. V., Nathan, G. J., Kelso, R. M. and Mi, J., Low kinetic-energy loss oscillating-triangular-jet nozzles, *Experimental Thermal and Fluid Science*, **27**, 2003, 553–561.

[4] Mi, J., Nathan, G. J., Luxton, R. E. and Luminis Pty. Ltd., *Naturally Oscillating Jet Devices*, Australian Patent Office, Application No.: PP0421/97, 1998.

[5] Nathan, G. J., Hill, S. J. and Luxton, R. E., An axisymmetric 'fluidic' nozzle to generate jet precession, *Journal of Fluid Mechanics*, **370**, 1998, 347–380.

[6] Newbold, G. J. R., Nathan, G. J., Nobes, D. S. and Turns, S. R., Measurement and prediction of NO_X emissions from unconfined propane flames from turbulent-jet, bluff-body, swirl, and precessing jet burners, in *Proceedings of the Combustion Institute, Volume 28*, 2000, 481–487.

[7] Rapson, D., Stokes, B. and Hill, S. J., Kiln flame shape optimisation using a Gyro-Therm gas burner, *World Cement*, **26**(7), 1995, 2–5.

[8] Schram, C., Rambaud, P. and Riethmuller, M. L., Wavelet based eddy structure eduction from a backward facing step flow investigated using particle image velocimetry, *Experiments in Fluids*, **36**, 2004, 233–245.